NUMERICAL SIMULATION ON ANISOTROPIC SQUEEZING PHENOMENON OF NEW GUANYIN TUNNEL

Tai-Tien Wang [1] and Tsan-Hwei Huang [2]

ABSTRACT

The strength and deformability anisotropy of rock masses caused by discontinuities is highly complicated in analysis and design of rock engineering. As the excavation sequence and support systems during tunneling cannot control deformation of surrounding rock in time, anisotropic squeezing behavior may occur and make tunneling very difficult. This study uses a numerical model that considers both elasto-plastic behavior and time-dependent deformation of rock masses to investigate the squeezing phenomenon in the New Guanyin Tunnel, Taiwan. The effects of discontinuities on surrounding rock deformation of a tunnel are discussed, and the mechanism and associated mobilization of squeezing phenomenon are elucidated.

Key words: Rock tunnel, anisotropic deformation, time-dependent deformation, squeezing.

1. INTRODUCTION

Squeezing phenomenon is the time-dependent large deformation during tunneling. Significant squeezing deformation of surrounding geomaterials may lead to insufficient clearance, support failure, reveling or even collapse of the tunnel; resulting in construction time delay and project cost increase. Squeezing problem has become one of the major obstacles for a tunnel excavated in high overburden area or underwent unfavorable geological situations (Barla 1995; Bhasin and Grimstad 1996; Weng *et al*. 2010).

The excess deformation and associated time-dependent behavior of a squeezing tunnel is influenced by not only the deformational characteristics of intact rock, but also the discontinuities that separate the intact rock and ubiquitously exist in a jointed rock mass. Existing models can either handle the pre- or post-peak deformation of intact rock or discontinuities alone; however, it is still troublesome to simulate the time-dependently anisotropic deformation of a tunnel.

Deformations of rocks surrounding the New Guanyin Tunnel exhibited asymmetric characteristics due to the influence of discontinuities. In several positions, tunneling was hindered by the need to construct reinforcements that support potential failure areas. Finally, a cave-in was induced by this asymmetrical dime-dependent deformation (United Geotech, Inc. 2001; Wang *et al*. 2002). This study utilizes a numerical model that considers both elasto-plastic behavior and time-dependent deformation of rock masses to investigate the squeezing phenomenon. The effects of discontinuities on surrounding rock deformation of a tunnel are discussed, and the mechanism and associated mobilization of squeezing phenomenon are elucidated.

Manuscript received May 4, 2011; revised October 2, 2011; accepted October 7, 2011.

[1] Associate Professor (corresponding author), Institute of Mineral Resources Engineering, National Taipei University of Technology, Taipei 10608, Taiwan, R.O.C. (e-mail: ttwang@ntut.edu.tw).

[2] Professor, Department of Civil Engineering, National Taiwan University, Taipei 10617, Taiwan, R.O.C. (e-mail: thhuang@ntu.edu.tw).

2. SQUEEZING PHENOMENON

The New Guanyin Tunnel, located in eastern Taiwan, is 10,307 m long. The tunnel is a typical double-lane railway tunnel 9.1 m wide and 7.3 m high. To reduce construction time, both portals and two adits, *i.e.*, the south and north adits, were arranged for tunnel excavation. The north adit and later the north working face of main tunnel ran into squeezing rock, resulting in significant tunnel deformation and support failure (Fig. 1). The squeezing phenomenon in the section from Station 28 k + 285 to 28 k + 220 is discussed as follows.

2.1 Engineering Geology

The New Guanyin Tunnel, which is located in the eastern foothill of the Central Mountain Range, goes through the mountain at roughly 1,300 m in height and is aligned parallel to the coastline bordering the Pacific Ocean. The Tananao Formation in this area is mainly composed of mica schist intercalated with chlorite schist, calcite schist and limestone. Rock strength ranges from weak to medium. However, the well-developed schistosity and joints and the high ground water level lead to difficulty during tunneling.

United Geotech, Inc., (2001) reported that the swelling potential of surrounding rock in this area was very low, classifying the rock mass into types IV and V using the rock mass classification method. Based on the Geological Strength Index (GSI) proposed by Hoek and Brown (1997), the structure of a rock mass can be classified as “block/disturbed”, and the surface condition is from “fair smooth” to “very poor.” The GSI is 10-45. Figure 2 shows the engineering geological map between Stations 28 k + 220 ~ 28 k + 280, that is summarized from the geological records of tunnel working face.

2.2 Tunnel Construction and Squeezing Phenomenon

The top heading method was applied in the studied section by machinery excavation. Drilling and blasting was also carried out occasionally to remove hard rock. The support system comprised H-125, H-150 and H-200 sectional steel ribs, 0.15-0.20 m thick shotcrete with steel mesh and 4-9 m long rockbolts.

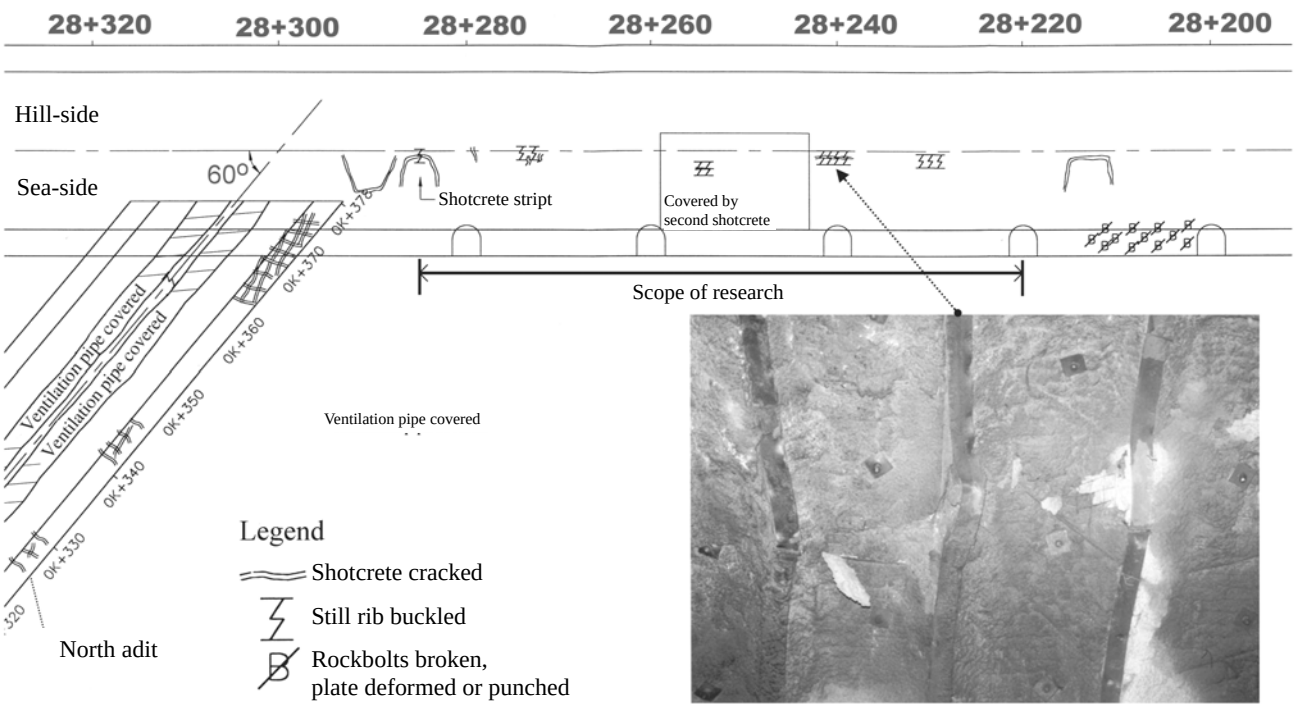

Fig. 1 Squeezing phenomenon happened in New Guanyin Tunnel

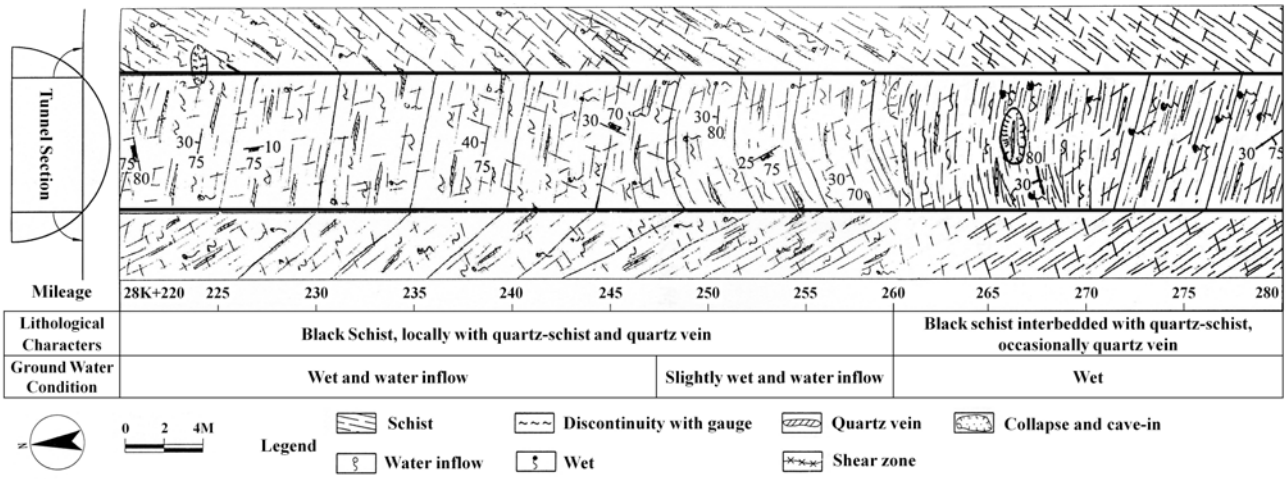

Fig. 2 Engineering geological map between Stations 28 k + 220 ~ 28 k + 280

Deformation of rock surrounding the tunnel was significant following crown excavation, but did not have a tendency for convergence. Once the bench was excavated, the deformation existed for several months. In many sections, the convergence, neglecting the deformation happened before the installation of monitoring instrumentation, reached approximately 2.0% compared with the tunnel diameter. The tunnel experienced the squeezing phenomenon in evidence.

Reinforcements were carried out before long to suppress the deformation of surrounding rock. Cement grouting, secondary shotcrete, long rockbolts, U-type sectional steel ribs and footing concrete were used. The deformation was eventually controlled. However, shotcrete cracking and punching failure at the bearing plate of rockbolts, broken rockbolts and buckled steel ribs were common in this tunnel section (Fig. 1).

3. CONSTITUTIVE LAW AND NUMERICAL MODEL

Wang and Huang (2006; 2009) developed a three-dimensional non-linear constitutive model and an associated two-dimensional numerical implementation for a rock mass with regularly distributed ubiquitous joint sets. The model combines the mechanical behavior of intact rock, the spatial configuration of joint sets, and mechanical behavior of the joint plane into the rock mass using representative volume elements. Thus, this model can characterize joint-induced anisotropy in terms of strength and deformation of a rock mass.

3.1 Constitutive Model

Assemblage for Deformation of an Ubiquitous Jointed Rock Mass

A rock mass with a unit volume consisting of M sets of ubiquitous joints, as shown in Fig. 3, under a uniform stress state $\boldsymbol{\sigma}$ is considered. Three parameters, *i.e.*, the strike β, the dip γ and the spacing S, allocate the spatial configuration of each joint set. When subjected to a small increment of stress $\mathbf{d\sigma}$, the corresponding incremental strain of the rock mass is $\mathbf{d\varepsilon}$. The incremental strains typically consist two components–one from the intact rock deformation $\mathbf{d\varepsilon}^I$, and the other by deformations of M sets of joints, $\mathbf{d\varepsilon}^J$. Thus,

$$\mathbf{d\varepsilon} = \mathbf{d\varepsilon}^I + \mathbf{d\varepsilon}^J \tag{1}$$

Before the applied load reaches peak strength, $\mathbf{d\varepsilon}^I$ can be expressed in terms of the compliance matrix of intact rock $\mathbf{C}^I$, as

$$\mathbf{d\varepsilon}^I = \mathbf{C}^I \mathbf{d\sigma} \tag{2}$$

For a unit volume of the rock mass, deformation of the total M sets of joints $\mathbf{d\varepsilon}^J$ is related to the constitutive relation $\mathbf{D}^\alpha$, the transformation matrix $\mathbf{L}^\alpha$, and the area projection matrix $\mathbf{B}^\alpha$ of the α-th joint plane, and can be derived as

$$\mathbf{d\varepsilon}^J = \sum_{\alpha=1}^{M} \frac{1}{S^\alpha} \mathbf{B}^{\alpha T} \mathbf{L}^{\alpha T} \mathbf{D}^\alpha \mathbf{L}^\alpha \mathbf{B}^\alpha \mathbf{d\sigma} \tag{3}$$

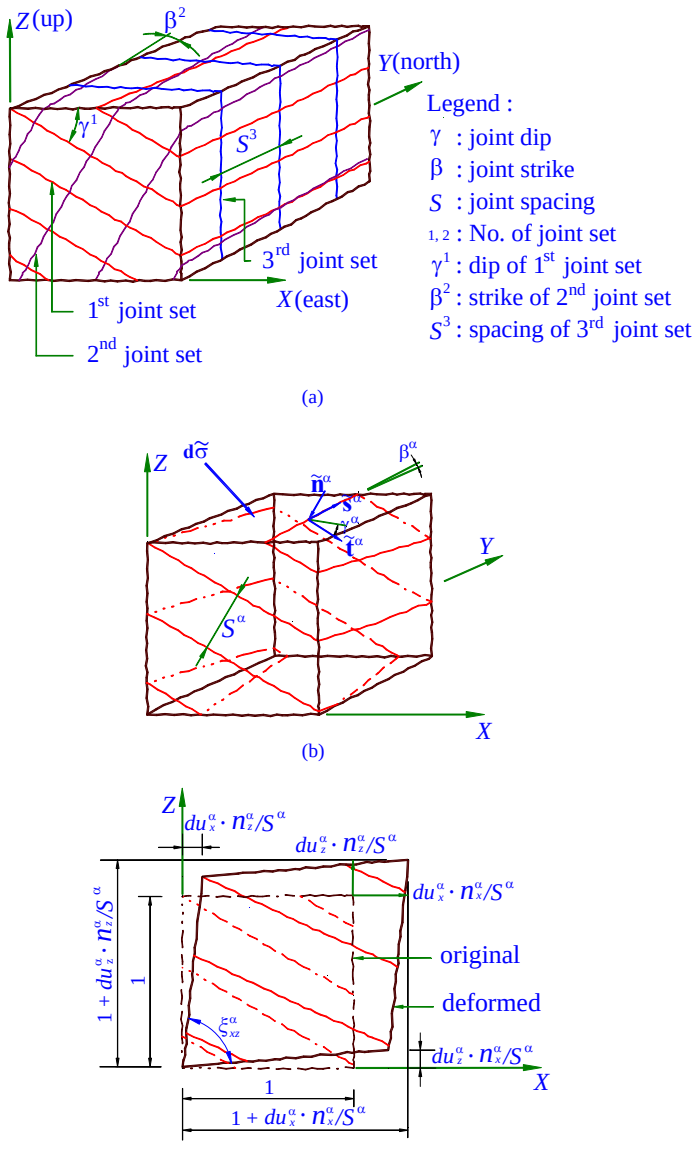

Fig. 3 Configuration of multi-sets of ubiquitous joints in rock mass; (a) Three parameters, *i.e.*, the strike β, the dip γ and the spacing S, allocate the spatial configuration of each joint set; (b) Configuration of 3-D rock mass with unit length in all sides and containing the α-th joint set for a particular set of joints considered. A local coordinate for each joint set is defined; (c) Deformation in *XZ*-plane associated with the deformation of the α-th joint set (Wang and Huang 2009)

Equation (3) can be rewritten as $\mathbf{d\varepsilon}^J = \mathbf{C}^J\ \mathbf{d\sigma}$, where $\mathbf{C}^J = \sum_{\alpha=1}^{M} \frac{1}{S^\alpha} \mathbf{T}^{\alpha T} \mathbf{D}^\alpha \mathbf{T}^\alpha$ represents the compliance matrix of all joint sets, and $\mathbf{T} = \mathbf{LB}$. The $\mathbf{D}^\alpha$ is a three by three compliance matrix associated the joint plane and has nine entries corresponding to the three axes of local coordinates (***n***, ***s***, and ***t***) for this particular set of joints, as shown in Fig. 3(b). However, only three independent elements (D_{ss}, D_{ns} and D_{nn}) of the compliance matrix are considered here. The empirical relation, which utilizes initial normal stiffness k_{ni} and maximum closure u_n^m, proposed by Bandis *et al.* (1983) are utilized to determine D_{nn} under various stress state. The mobilization of the *JRC* during shearing, proposed by Barton *et al.* (1985), is used to determine D_{ss} and D_{ns} corresponding to various shearing levels. The transformation matrix, $\mathbf{L}^\alpha$, is composed of directional cosines between local coordinates ($\boldsymbol{n}^\alpha$, $\boldsymbol{s}^\alpha$, and $\boldsymbol{t}^\alpha$) and global coordinates (*X*, *Y*, and *Z*). Additionally, $\mathbf{B}^\alpha$ is a matrix representing the area projection of the α-th joint plane onto the *Y*-*Z* plane, *Z*-*X* plane, and *X*-*Y* plane.

Failure Modes and Strength Criteria

For a specific representative volume element, three failure modes are considered and incorporated into the adopted model (Wang 2003); these three failure modes are (1) tensile failure of intact rock, (2) shear failure of intact rock and (3) joint sliding.

The conventional Mohr-Coulomb failure criterion with peak friction angle, ϕ_p, peak cohesion, c_p and tensile strength, σ_t, of intact rock is adopted as the failure criterion for intact rock. Barton's empirical formula is used to estimate the shear strength of joint plane and as the failure criterion of joint sliding through three parameters-joint roughness coefficient, *JRC*, uniaxial compressive strength of a joint wall, *JCS*, and its basic friction angle, ϕ_b.

The applied stress state dominates the failure mode of a rock mass. Prior to failure, existing stress σ is updated by adding $\mathbf{d\sigma}$ computed from the previous loading step. The updated stress state is checked to determine whether it reaches the failure criteria in turn. Additionally, tensile normal stress leads to joint opening, which cannot sustain tension, and the local stress will be redistributed to the surrounding rock mass.

Following the above-mentioned processes, either intact rock failure or joint sliding failure along any joint set can be identified, and, accordingly, the strength of the rock mass can then be determined. Once failure mode is determined the corresponding post-peak deformation can be determined, as in the following section.

Post-Peak Deformation

The stress-strain relationship of intact rock before and after failure can be respectively described by Eq. (2) and plasticity theories. If strain softening or hardening occur, the plasticity normality rule can be used to describe the development of the yield/failure surface. These methods are adopted in the model used.

For each set of joints, only element D_{ss} in Eq. (3) involves post-peak deformation, which can be described using the mobilization of *JRC* during shearing proposed by Barton *et al.* (1985). As such, deformation behaviors adopted in the model are mainly based on published results and commonly used in engineering practice. The model combines these behaviors, such that a sophisticated deformation model capable of describing anisotropic pre- and post-peak deformation and strain softening/hardening is established accordingly (Wang 2003).

3.2 Numerical Implementation

Wang and Huang (2009) incorporated the above-mentioned constitutive model for a two-dimensional rock mass into a subroutine for the explicit finite difference software program, FLAC. Through the numerical implementation, the adopted constituted model can be utilized to simulate a practical engineering task in a rock mass containing sets of ubiquitous joints with the following features.

1. The failure modes corresponding to stress conditions, which inherently determine anisotropic strength, can be selected automatically.
2. The major properties of joints, such as closure, shear and the associated dilatancy of joints, can be considered in the stress-strain relationship.
3. The progressive failure, which results in strain softening of a rock mass, can be described in post-peak deformation.

The numerical implementation for the adopted constitutive model has been verified through a series of comparisons between its predictions to the results of existing models and laboratory experiments (Wang 2003; Wang and Huang 2009).

Furthermore, the analytical solution for deformation of a rock mass containing orthogonal joint sets proposed by Amadei and Goodman (1981) is utilized to validate the application of the adopted model for tunnel excavation. Excavation-induced displacement surrounding a tunnel in a rock mass with two orthogonal joint sets is considered. Table 1 lists the input parameters for the validation. Figure 4 shows the distribution of rock displacement simulated by the adopted model and associated comparison with the analytical solution. Both the simulated horizontal and vertical components of displacement (u_x and u_y) match each other with the maximum error of 1.2% (Fig. 4(b)). The adopted model is able to simulate anisotropic deformation surrounding a tunnel in jointed rock masses.

3.3 Time-Dependent Deformation

Using a visco-elastic- or a visco-plastic constitutive model, the time-dependent deformation of a tunnel excavated in a rock mass can be simulated. However, a model which can describe the time-dependent deformation, and meanwhile, simulate the anisotropic pre- and post-deformation of rock mass with multi-sets of joints, is not yet available. As such, the approach proposed by Aydan *et al.* (1996) is used in this manuscript. The time-dependent behavior of rock is correlated with its uniaxial compressive strength corresponding to various stages and expressed as

$$\frac{\sigma_c^c}{\sigma_c^0} = \frac{\sigma_c^\infty}{\sigma_c^0} + \left[1 - \frac{\sigma_c^\infty}{\sigma_c^0}\right] \mathrm{e}^{-t/\omega} \tag{4}$$

where σ_c^0 and σ_c^∞ are the short term and the ultimate uniaxial compressive strength of rock, respectively, ω is the retardation time to failure, σ_c^c is the uniaxial compressive strength corresponding to time *t*. The uniaxial compressive strength of rock corresponding to various stages can be determined by laboratory tests or from back analysis.

Table 1 Parameters for validation of a circular tunnel excavated in a rock mass containing two sets of orthogonal joints

Intact rock		Joints		
			Set I	Set II
Elastic modulus E (GPa)	10.0	Dip γ (°)	0.0	90.0
		Spacing S (m)	1.0	0.1
Poisson's ratio	0.25	Normal stiffness K_{nn} (GPa/m)	20.0	20.0
		Shear stiffness K_{ss} (GPa/m)	5.0	5.0

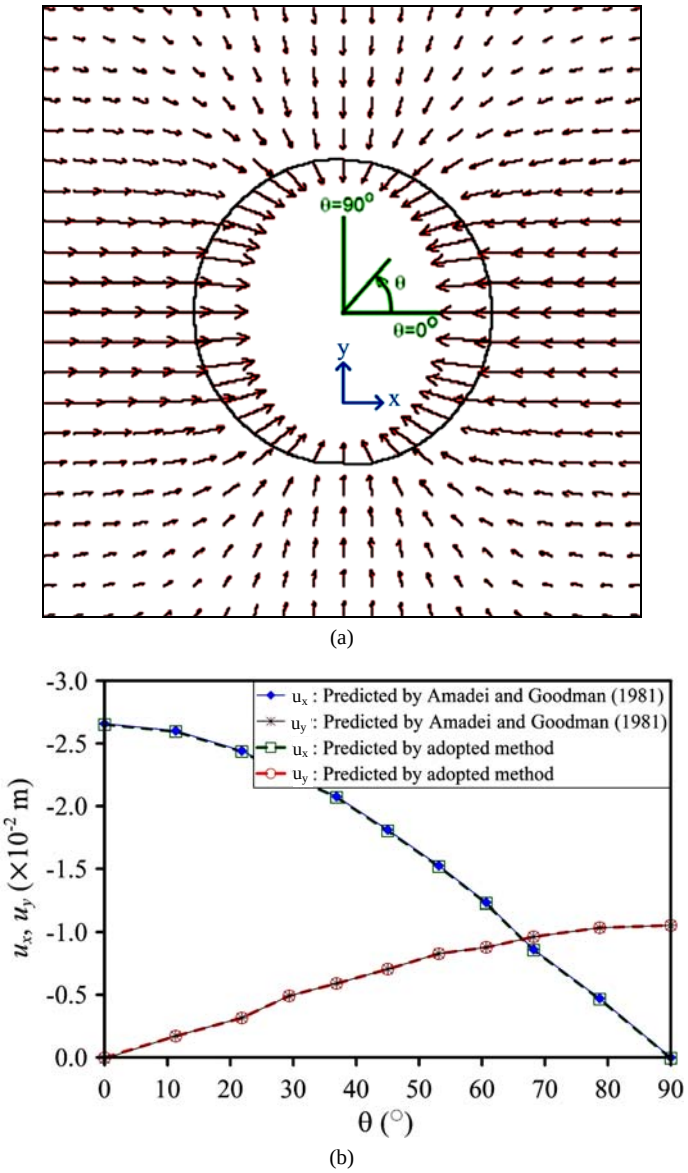

Fig. 4 (a) Distribution of rock displacement simulated by the adopted model and (b) associated comparison with the analytical solution

Table 2 Parameters for time-dependent deformation validation of Taw Tunnel (Aydan *et al.* 1996)

Elasto-plastic part		Time-dependent part	
Peak cohesion c_p (MPa)	1.99	Ratio of ultimate- to short term uniaxial compressive strength $\sigma_c^{\infty}/\sigma_c^{0}$ (%)	60
Peak friction angle ϕ_p (°)	32.87	Ultimate uniaxial compressive strength σ_c^{∞} (MPa)	4.38
Bulk modulus K (MPa)	1123		
Poisson's ratio	0.31	Retardation failure time ω (days)	500

Table 2 lists parameters of Taw Tunnel reported by Aydan *et al*. (1996). Using the adopted model and the parameter listed in Table 2, the time-dependent deformation of the tunnel is simulated and thus compared with the analyzed results of Aydan *et al*. (1996) (Fig. 5). The maximum error is 2.5%. The adopted model simulates the time-dependent deformation surrounding the Taw Tunnel well.

4. SIMULATION RESULTS AND DISCUSSION

4.1 Numerical Simulation

Two dimensionally numerical analysis is used to simulate tunnel excavation and support installation. Tunneling sequences during top heading, installation of steel ribs, shotcrete and then rockbolts are simulated in a step-by-step manner. Long bench excavation matches the situation at the site. Beam and cable elements are utilized to simulate the support effects of shotcrete and rockbolts, respectively. Figure 6 presents the simulation procedure for numerical analysis. Furthermore, the pre-deformation occurred prior to support installation is also considered in the analysis. Based on the closure formula developed by Sulem *et al*. (1987), the ratio of pre-deformation to total deformation is 18.4-33.3% by measured data regression. The support elements are installed until the maximum rock deformation surrounding the tunnel reaching the ratio to total deformation.

According to the geological survey of the working face, one set of schistosity and three sets of joint present in this section. Table 3 presents the attitudes, persistency and spacing of these discontinuities. As each set of discontinuities have small discrepancies, average values are used for simplicity sake. A stereographic projection is used to identify the representative apparent dips for two-dimensional analysis. Joint set *C* is ignored in the analysis as it is only exposed at limited few sections. Persistency of the other discontinuities is assumed such that the joint sliding would not be affected. Table 4 lists the parameters of intact rock and discontinuities used in analysis. The strain softening behavior is considered and the associated flow rule is used. The strength parameters are decreased with the plastic strain ε^p to yield a residual strength equaling 2/3 of peak strength at $\varepsilon^p = 3\%$.

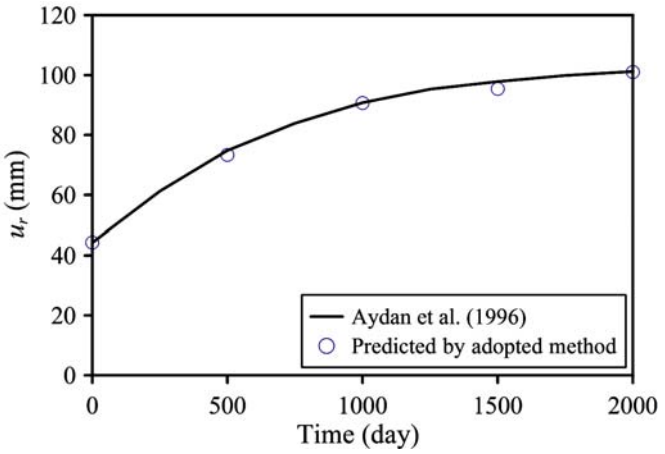

Fig. 5 Comparison of time-dependent radial deformation u_r simulated by the adopted model and analyzed results of Aydan *et al.* (1996)

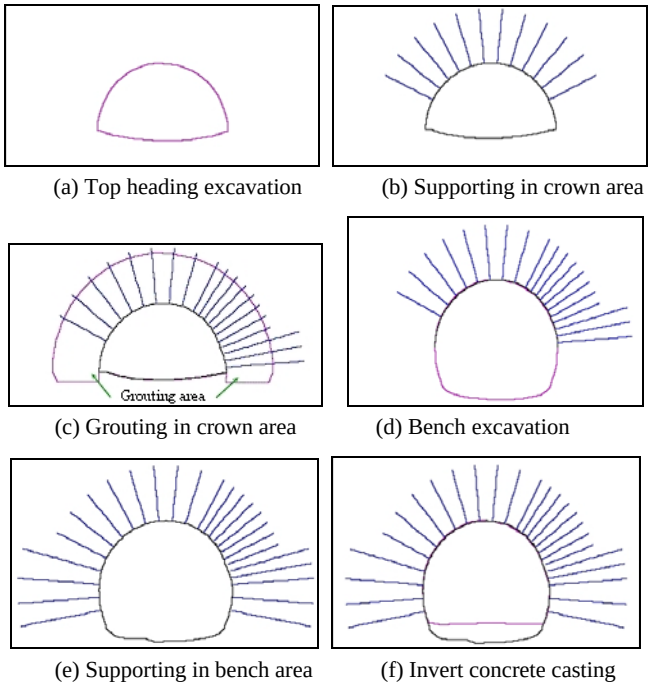

(a) Top heading excavation (b) Supporting in crown area

(c) Grouting in crown area (d) Bench excavation

(e) Supporting in bench area (f) Invert concrete casting

Fig. 6 Procedure of numerical simulation on squeezing section

The studied area are more than 300 m away from the slope surface and the surrounding rock deformations neighboring to the area are approximately symmetric to the center line of the tunnel. Consequently, we assume that the vertical stress component is equal to the overburden stress and the lateral earth pressure coefficient is 1.0. Vertical and horizontal stresses are −5.98 MPa in this analysis.

A mesh with a size of 160 m × 160 m and an element number of 5184 is then established. The sizes of the elements are mutative with a minimum size of 0.7 m × 0.7 m in the center part. All boundaries of the mesh are set to be fixed ones.

4.2 Results and Discussion

In the early stages of tunneling, *i.e.*, the working face advanced away from the monitoring station a distance roughly two

Table 3 Attitudes, persistency and spacing of discontinuities

Item	Schistosity	Joint A	Joint B	Joint C
Strike (°)	N50 ~ 55W	N0 ~ 40W	N50 ~ 80W	N0 ~ 40W
Dip (°)	40 ~ 50N	60 ~ 80WS	40 ~ 80WS	60 ~ 80EN
Spacing (m)	—	0.1 ~ 1.5	0.2 ~ 0.5	0.2 ~ 0.5
Description	Intercalated with quartz and gouge occasionally, truncated by joint, poor persistency	Opening width less than 3 mm, uneven, persistency ranges between 0.2 ~ 4.0 m	Opening width ranges between 3 ~ 10 mm, uneven, persistency ranges 1.0 ~ 4.0 m	Exposed range less than 4 m, opening width less than 3 mm, uneven

Table 4 Parameters used for intact rock and discontinuities

Intact rock		Discontinuities	Schistosity	Joint A	Joint B
Peak cohesion (MPa)	12.2	Apparent dip (°)	36	–69	–45
Peak friction angle (°)	38.0	Spacing (m)	0.1	0.8	0.35
Bulk modulus (MPa)	8333	*JRC*	20	12	8
Poisson's ratio	0.2	*JCS* (MPa)	31.0	31.0	31.0
		Basic friction angle (°)	37.0	35.0	33.0
Uniaxial compressive strength (MPa)	31.0	Initial normal stiffness (GPa/m)	50.0	20.0	10.0
		Maximum closure (m)	1.0E-4	1.0E-3	2.0E-3

Remark: Ultimate uniaxial compressive strength is assumed to be 60% of its short term strength, retardation failure time is assumed to be 150 days

to three times of tunnel diameter, Fig. 7(a) presents the deformation vector of surrounding rock. Figure 8(a) presents the failure zone, characterized by intact rock failure and joint sliding. Due to the presence of schistosity and joints, the deformation vectors in the sea-side (right side in Fig. 7(a)) wall and in the connection area of the temporarily invert and hill-side wall are significantly greater than those at other locations. The failure zone is roughly 1-3 m thick at the crown, and is 3-5 m thick at the bench area due to decreased support stiffness and low support strength (Fig. 8(a)). The marked displacement of surrounding rock and stress concentration effect bring about that the shotcretes in the sea-side wall and both footing areas reached plastic moment (Fig. 9(a)). The rockbolts in the vault also fail locally because of insufficient bonding strength (Fig. 9(b)).

The parameters listed in Table 4 are adopted to simulate the time-dependent deformation of rock surrounding the tunnel. Figures 7(b) and 7(c) present variations of deformation magnitudes and associated horizontal and vertical component around tunnel wall, and Figure 8(b) the failure zone 60 days after tunneling. Compared with Figs. 7(b) and 7(c), deformations increased on sea-side wall up to 0.2 m, especially at $\theta = 20°$, and were unapparent at the crown ($\theta = 90°$) and on the hill-side wall ($\theta = 150$ - $180°$). The failure zone extended to 4-5 m and resulted in support failure in the sea-side wall and crown (Figs. 9(c) and 9(d)), which coincides with the site condition shown in Fig. 1.

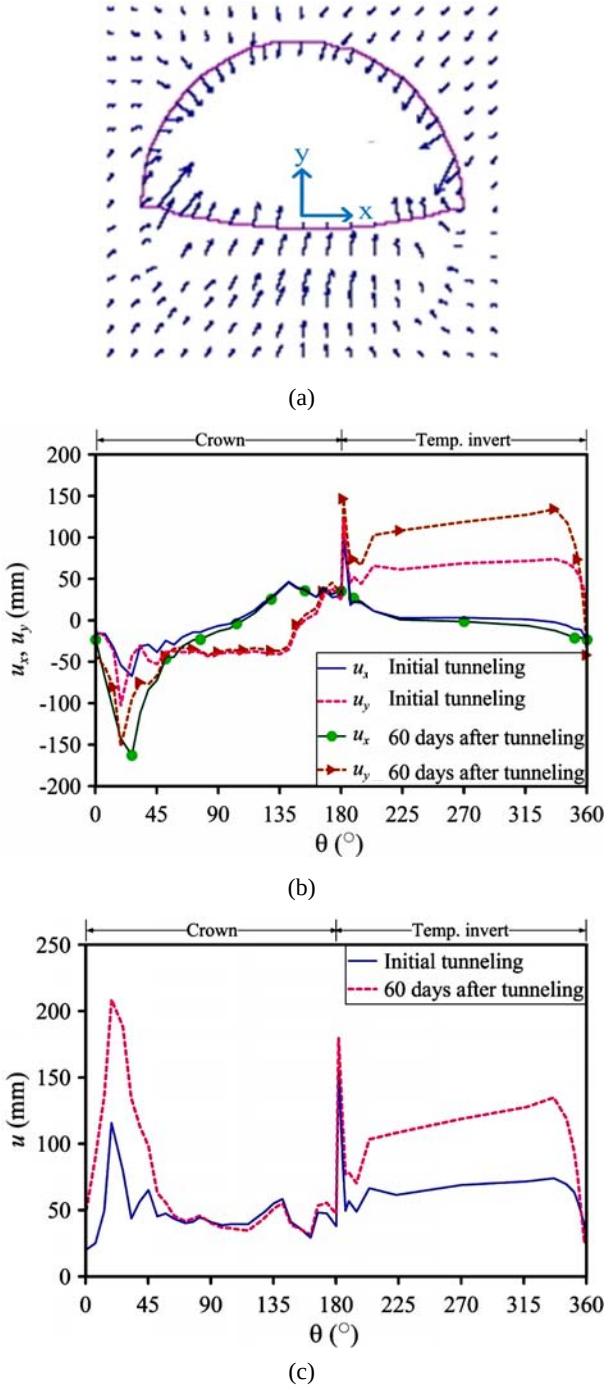

Fig. 7 Variation of simulated deformation; (a) Deformation vector at early stage of tunneling; (b) Horizontal and vertical components of deformation vectors; (c) Magnitude of deformation vectors

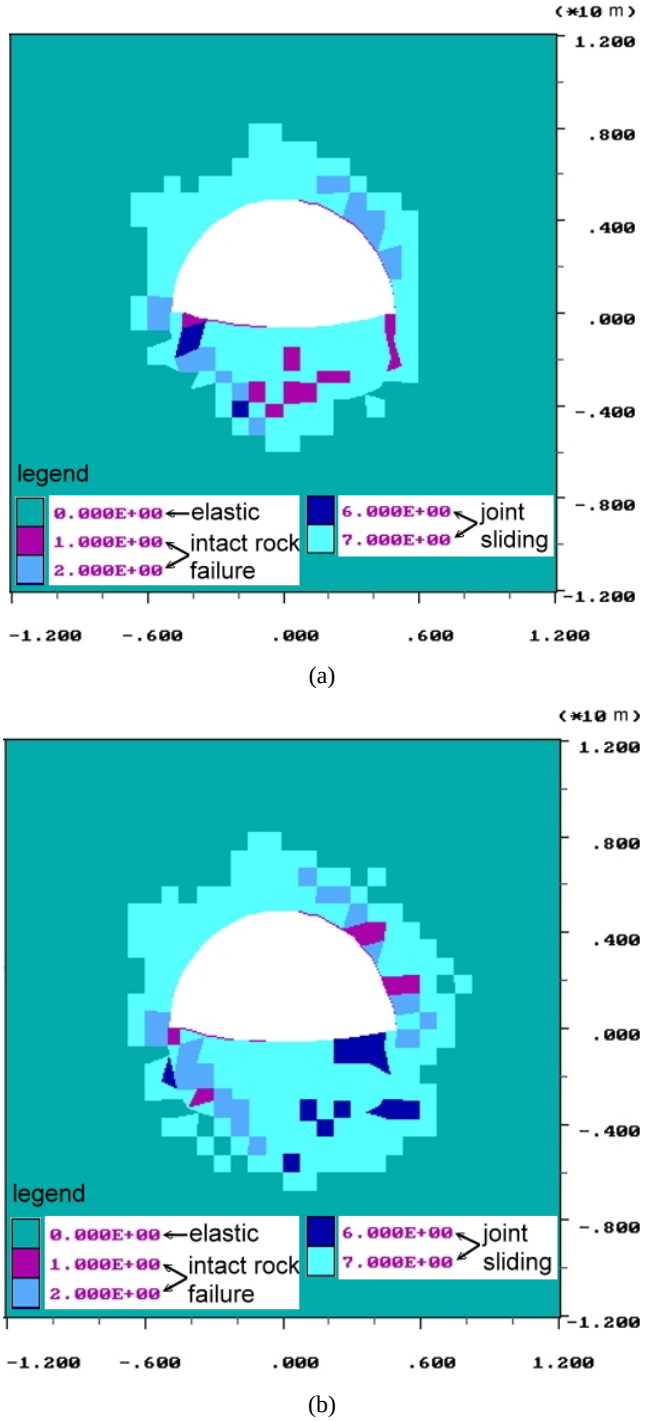

Fig. 8 Failure zone in (a) the early stage of tunneling and (b) 60 days after tunneling. The *x*, *y* coordinates present scales in units of meter.

Figure 9 shows the variation of support stresses. At early stage of tunneling, large displacement of surrounding rock and stress concentration effect in right (sea-side) wall and both footing area bring about the plastic moment of shotcrete, and the rockbolt in vault also fails locally because of insufficient bonding strength. Sixty days after tunneling, the time-dependent rock deformation increases the support stress. Significant area both in crown and in temporary invert where the shotcrete reaches its plastic moment and the rockbolts stress/strength ratio is 1 can be observed. The anisotropic squeezing induced tunnel support failure is obvious and again fit in with site condition shown in Fig. 1.

Figure 10 compares the simulated tunnel convergence with measurement results. Both the raw data and the pre-deformation modified historical convergence curve are plotted. The difference between measured and calculated data is far less than the modification amount for pre-deformation. Additionally, the asymmetrical deformation caused by the presence of discontinuities is reflected in D1 and D2 convergence curves.

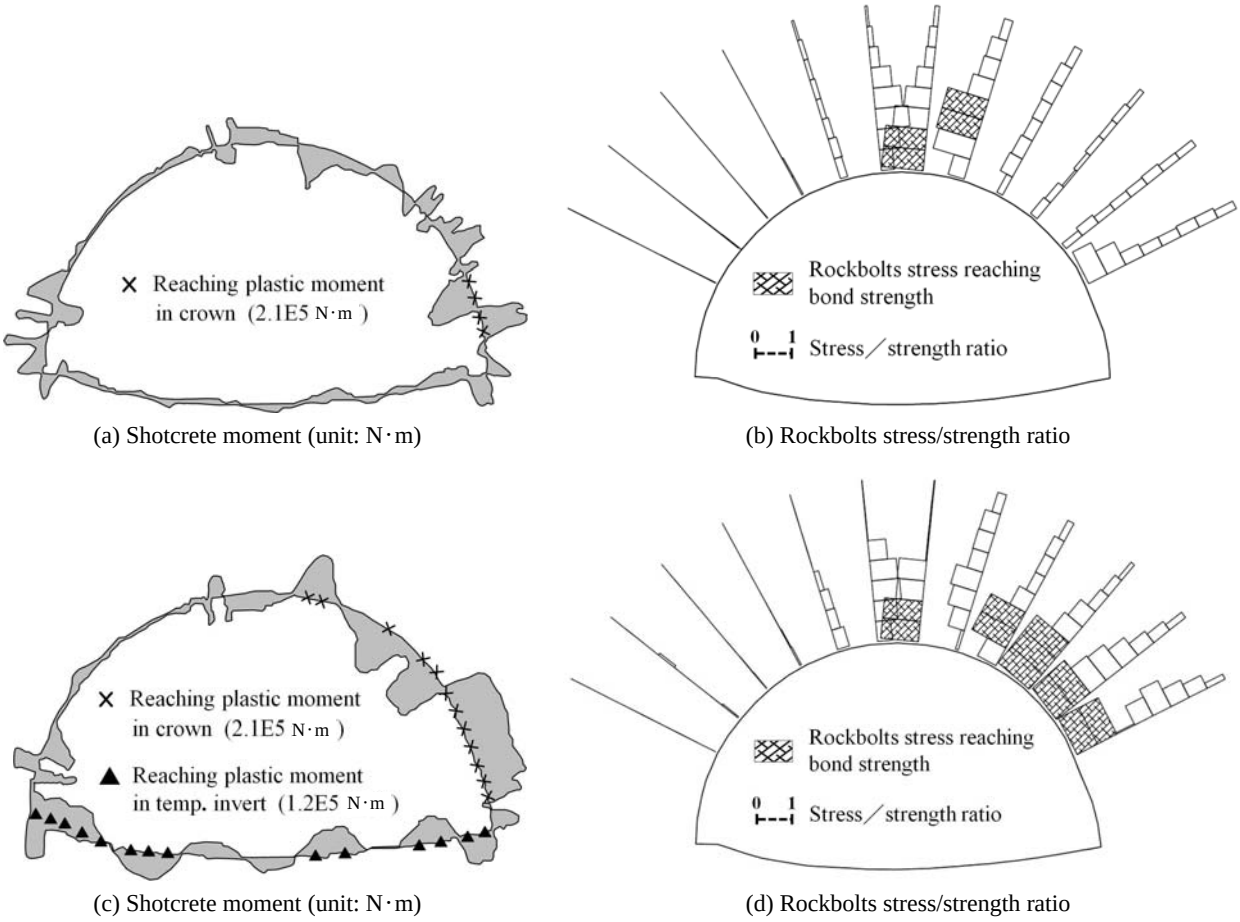

(a) Shotcrete moment (unit: N·m)

(b) Rockbolts stress/strength ratio

(c) Shotcrete moment (unit: N·m)

(d) Rockbolts stress/strength ratio

Fig. 9 Simulated variation of support stresses; (a) Moment of shotcrete in the early stage of tunneling; (b) Rockbolts stress/strength ratio in the early stage of tunneling; (c) Moment of shotcrete 60 days after tunneling; (d) Rockbolts stress/strength ratio 60 days after tunneling

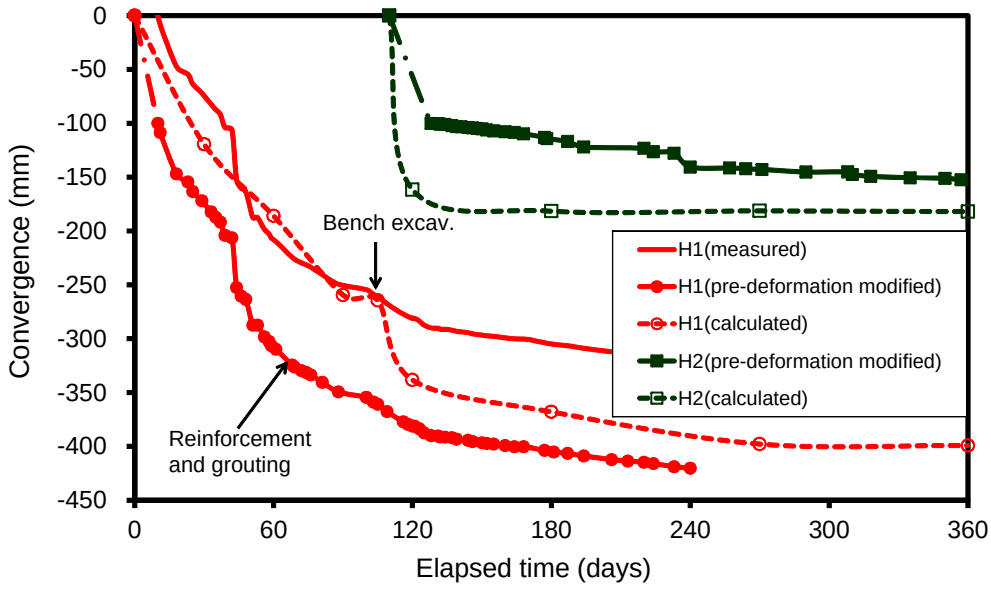

(a) H1 and H2 convergence

Fig. 10 Comparison of simulated results and measured data

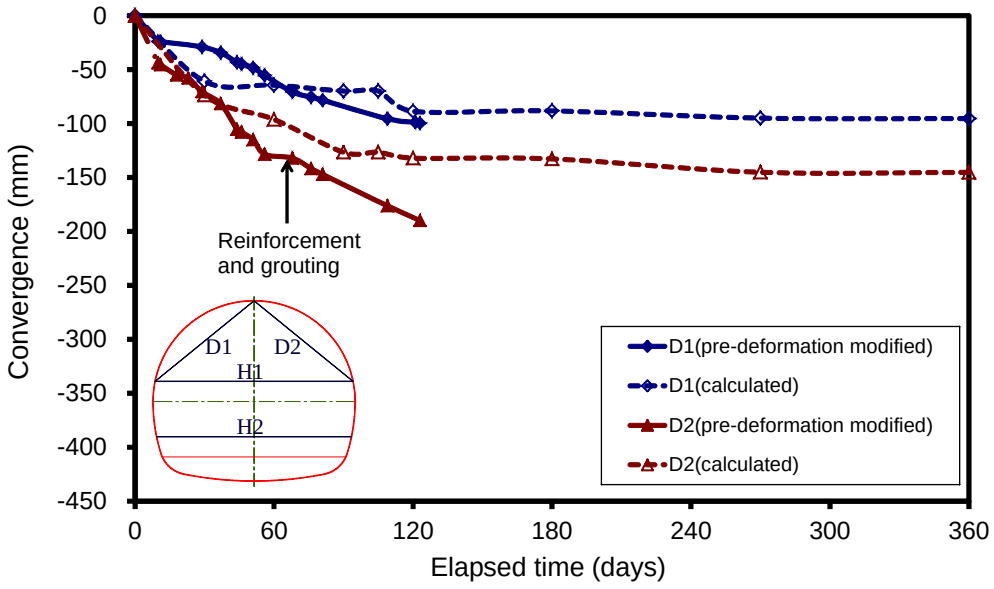

(b) D1 and D2 convergence

Fig. 10 (continued)

5. CONCLUSIONS

Application of the mechanical and associated numerical model proposed by Wang and Huang (2009) to the New Guanyin Tunnel indicates that discontinuities comprise an important factor affecting the tunneling behavior. The well-known stresses varying around a tunnel, *i.e.*, unloading in a radial direction and loading in a tangential direction, may cause shear failure or tensile failure of intact rock. This stresses varying also decreases the normal force and increases the shear force on some discontinuities with normal vectors parallel and sub-parallel to the radial direction of the tunnel. Shear strength of these discontinuities decreased accordingly, and may result in failure, *i.e.*, joint sliding, prior to discontinuities with other directions. In case many sets of joints presence, the failure zone will be superposed one another and significantly increase tunnel convergence. Intact rock and joints typically exhibit strain-softening post-peak behavior, and their mechanical properties are strain-softening and post-peak behavior. As the excavation sequence and support systems during tunneling cannot control deformation of surrounding rock in time, the squeezing phenomenon may initiate and induce significant time-dependent anisotropic deformation.

ACKNOWLEDGEMENTS

The authors would like to thank the National Science Council, Taiwan, for financially supporting this research under Contract Nos. NSC 97-2621-M-027-003 and NSC 99-2628-E-027 –006.

REFERENCES

Amadei, B. and Goodman, R. E. (1981), "A 3-D constitutive relation for fractured rock masses." *In: Proc. Int. Symp. Mech. Behavior Structured Media*, Ottawa, 249-268.

Aydan, Ö., Akagi, T., and Kawamoto, T. (1996), "The squeezing potential of rock around tunnels: Theory and prediction with examples taken from Japan." *Rock Mech. & Rock Engng.*, **29**(3), 125-143.

Bandis, S., Lumsden, A. C., and Barton, N. R. (1983), "Fundamentals of rock joint deformation." *Int. J. Rock Mech. Min. Sci. & Geomech. Abstr.*, **20**(6), 249-268.

Barla, G. (1995), Squeezing rocks in tunnels. News Journal, ISRM, **2**(3 & 4), 44-53.

Barton, N., Bandis, S., and Bakhtar, K. (1985), "Strength, deformation and conductivity coupling of rock joints." *Int. J. Rock Mech. Min. Sci. & Geomech. Abstr.*, **22**(3), 121-140.

Bhasin, R. and Grimstad, E. (1996), "The use of stress-strength relationships in the assessment of tunnel stability." *Tunnelling and Underground Space Technology*, **10**(1), 93-98.

Hoek, E. and Brown, E. T. (1997), "Practical estimates of rock mass strength." *Int. J. Rock Mech. Min. Sci. & Geomech. Abstr.*, **34**(8), 1165-1186.

Sulem, J., Panet, M., and Guenot, A. (1987), "Closure analysis in deep tunnels." *Int. J. Rock Mech. Min. Sci. & Geomech. Abstr.*, **24**(3), 145-154.

United Geotech, Inc., (2001). The Concluding Report on Site Engineering Geology Investigation and Evaluation Service of New Guanyin Tunnel, East Engineering Office of Railway Reconstruction Bureau, Ministry of Transportation and Communication, Taiwan.

Wang, T. T. (2003), *A Squeezing Model of Rock Tunnels*. Doctoral Dissertation of Department Civil Engineering, National Taiwan University, Taiwan.

Wang, T. T. and Huang, T. H. (2006), "Complete stress-strain curve for jointed rock masses." *ISRM Int. Symposium 2006/4th Asian Rock Mechanics Symposium*, Singapore, 283.

Wang T. T. and Huang, T. H. (2009), "A constitutive model for the deformation of a rock mass containing sets of ubiquitous joints." *Int. J. Rock Mech. Min. Sci.*, **46**(3), 521-530.

Wang, T. T., Wang, W. L., Xu, R. D., and Wang, G. Z. (2002), "Dealing with the tunnel squeezing nearby the intersection of north adit and new guanyin tunnel." *Modern Tunneling Technology*, Special Issue for 3rd Cross Straits Symposium on Tunneling and Underground Engineering, 293-299.

Weng, M. C., Tsai, L. S., Liao, C. Y., and Jeng, F. S. (2010), "Numerical modeling of tunnel excavation in weak sandstone using a time-dependent anisotropic degradation model." *Tunnelling and Underground Space Technology*, **25**, 397-406.